Journal of Power Sources 198 (2012) 23–29

Contents lists available at SciVerse ScienceDirect

Journal of Power Sources

journal homepage: www.elsevier.com/locate/jpowsour

# Development of supported bifunctional oxygen electrocatalysts and corrosion-resistant gas diffusion layer for unitized regenerative fuel cell applications

Sheng-Yang Huang, Prabhu Ganesan, Ho-Young Jung, Branko N. Popov*

*Center for Electrochemical Engineering, Department of Chemical Engineering, University of South Carolina, Columbia, SC 29208, USA*

ARTICLE INFO

*Article history:*
Received 25 August 2011
Received in revised form
21 September 2011
Accepted 22 September 2011
Available online 29 September 2011

*Keywords:*
Titania support
Bifunctional oxygen electrode
Corrosion resistance
Oxygen reduction reaction
Oxygen evolution reaction
Unitized regenerative fuel cell

ABSTRACT

A novel bifunctional oxygen electrode (BOE) consisting of titania supported electrocatalysts ($Pt/TiO_2$ and $Ir/TiO_2$) and a corrosion-resistant gas diffusion layer (GDL) were developed for application in unitized regenerative fuel cells (URFCs). The corrosion-resistant GDL comprised of a conventional carbon substrate and a protective micro-porous layer (MPL) of iridium–titanium nitride (Ir–TiN). Transmission electron microscopy (TEM) images revealed uniform distribution of Pt and Ir nanoparticles on the $TiO_2$ support with particle sizes of 4.5 and 2.0 nm, respectively, which was also confirmed by the XRD analysis. Among the various Pt–Ir compositions prepared, $Pt_{85}Ir_{15}$ (with a Pt/Ir weight ratio of 85/15) showed the highest catalyst efficiency towards oxygen reduction reaction (ORR) and oxygen evolution reaction (OER). The URFC testing results showed that the round-trip energy conversion efficiency ($\varepsilon_{RT}$) of supported $Pt–Ir/TiO_2$ (42%) was significantly higher than that of unsupported Pt–Ir black (30%). The $TiO_2$ support provided high surface area for the uniform dispersion of the catalyst particles. The URFC performance increase was ascribed to the uniform dispersion and better utilization of noble metal catalysts. Furthermore, the stability of URFC cycle performance was significantly improved by using Ir–TiN as an additional protective MPL mainly due to reduced carbon corrosion of the GDL especially during water electrolysis.



## 1. Introduction

A unitized regenerative fuel cell (URFC) is an electrochemical energy conversion and storage device that combines a fuel cell and a water electrolyzer in a single system [1–4]. It has the advantages of long-term energy storage over Li-ion secondary batteries and has theoretical energy density as high as 3660 Wh $kg^{-1}$ [5]. Despite their apparent advantages, URFCs are still in their early stages of development because of several limiting factors, including (a) performance and stability of the bifunctional oxygen electrode (BOE) [6,7], (b) carbon support corrosion [8,9], and (c) corrosion of gas diffusion layer (GDL) and bipolar plates [10–13].

The importance of the catalyst support has been well documented [8,14], i.e., (a) to provide high surface area over which small catalyst particles can be dispersed, (b) to allow mass transport to and from the active sites, and (c) to provide electronic conductivity within the catalyst layer. Carbon is the typical catalyst support material for PEM-based fuel cells due to its large surface area, high electrical conductivity, and well-developed pore structure. However, carbon corrosion is inevitable and disastrous at very high positive potentials (>1.5 V) when URFC is operated in the electrolyzer mode as indicated by the following reaction [15]:

$$C + 2H_2O \rightarrow CO_2 + 4H^+ + 4e^- \quad (E^o = 0.207\,\text{Vvs.NHEat25}\,^\circ\text{C}) \quad (1)$$

The high positive potentials during the oxygen evolution process set a practical limit on the lifetime of the supported catalyst. Currently, Pt and Ir black powders are being used as bifunctional oxygen electrode catalyst at significantly higher catalyst loadings [16–18]. However, the literature on supported BOE catalysts used for the URFC is limited and scarce [2,19,20].

The catalytic behavior of the catalyst in the BOE is affected by the size and composition of the metal nanoparticles, the interactions with the support, and the interactions between the metal components. The performance of the BOE varies significantly with the method used to prepare the electrode. Conventional methods such as adsorption, ion-exchange, or deposition of two metal precursors on the support often lead to the formation of metal particles that are relatively large and non-uniform in size and composition.

The carbon-based GDL employed in proton exchange membrane fuel cells (PEMFCs) cannot be used as such for URFC due to the carbon corrosion. Ioroi et al. [21] have reported titanium (Ti), which is a corrosion-resistive and electron-conductive material in highly cathodic and acidic environments, as the GDL for URFCs. Song et al. [10] have also reported that a protective micro-porous layer (MPL)

* Corresponding author. Tel.: +1 803 777 7314; fax: +1 803 777 8265.
*E-mail address:* popov@cec.sc.edu (B.N. Popov).

0378-7753/$ – see front matter © 2011 Elsevier B.V. All rights reserved.
doi:10.1016/j.jpowsour.2011.09.071

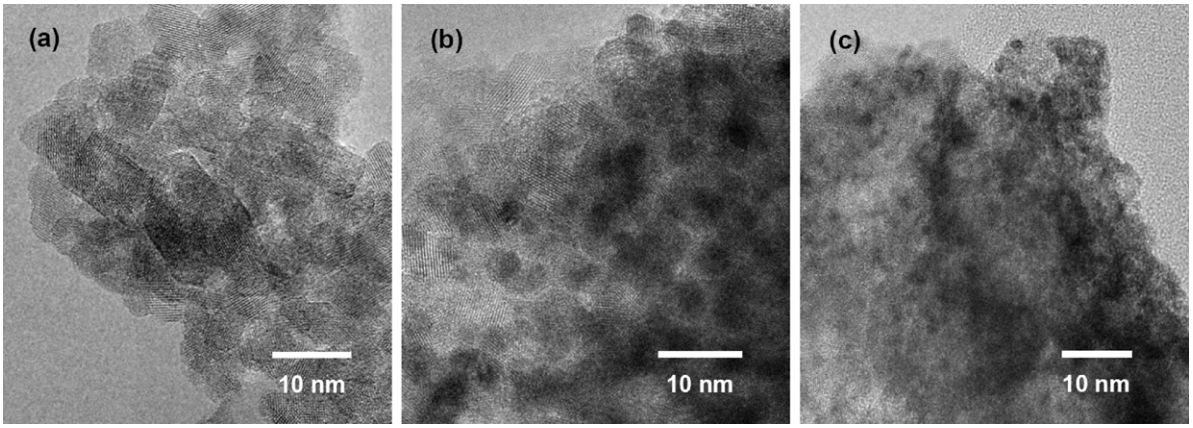


**Fig. 1.** The bright field TEM micrographs of (a) $TiO_2$, (b) $Pt/TiO_2$, and (c) $Ir/TiO_2$.

made of $IrO_2$/Ti as a corrosion-resistant GDL for URFC. Ir and $IrO_2$ can catalyze the active oxygen species rapidly to form the oxygen and reduce carbon corrosion of the GDL especially during water electrolysis.

In the present work, we report the synthesis of platinum and iridium catalysts supported on $TiO_2$ ($Pt/TiO_2$ and $Ir/TiO_2$) and preparation of a novel BOE utilizing $TiO_2$ supported electrocatalysts and Ir–TiN as a corrosion-resistant MPL. The aim of our study is to demonstrate that the synthesized electrocatalysts and the BOE exhibit better URFC performance and stability, together with high round-trip energy conversion efficiency. Our previous results showed that platinum catalyst supported on $TiO_2$ ($Pt/TiO_2$) exhibited higher fuel cell performance together with ultrahigh stability at high positive potentials [22]. In addition, we also show that titanium nitride (TiN) nanoparticles can be used as a microporous layer (MPL) material for preparing the GDL for URFC and can outperform the conventional carbon-based MPL in terms of stability and durability. TiN has higher electrical conductivity, comparable to that of carbon, and exceptional oxidation and acid corrosion resistance [23]. These unique properties have the potential to make TiN as a corrosion-resistant MPL for URFC application.

## 2. Experimental

### 2.1. Synthesis of $TiO_2$ and supported electrocatalysts

Mesoporous $TiO_2$ was synthesized by the controlled hydrolysis of titanium isopropoxide (Alfa Aesar) in the presence of a surfactant (Pluronic P123, BASF). The resulting white product was aged for 48 h. Subsequently, the surfactant embedded in the synthesized $TiO_2$ was removed by refluxing with hot water. For the preparation of the $Pt/TiO_2$ catalyst, a solution of $NaBH_4$ (Sigma–Aldrich), a deaerated suspension of the $TiO_2$ support and sodium dodecyl sulfate (Sigma–Aldrich), and a platinum precursor ($H_2PtCl_6$, Alfa Aesar) were prepared separately. The resulting three solutions were immediately mixed together and then stirred to allow the adsorption of the colloidal Pt particles onto the $TiO_2$ support. In order to achieve favorable electrical conductivity, catalysts with a metal loading of 60 wt% were prepared in this study. Supported iridium catalyst ($Ir/TiO_2$) was prepared using similar procedures at an elevated temperature. The resulting electrocatalysts were filtered and dried at 80 °C for 24 h. Finally, the electrocatalyst thus obtained was heat-treated in a tube furnace at 200 °C for 2 h under argon atmosphere to increase the interaction between catalyst particles and the $TiO_2$ support. Physical mixtures of $Pt/TiO_2$ and $Ir/TiO_2$ electrocatalysts with Pt:Ir compositions varying from 100:0 to 70:30 were prepared and used as BOE catalysts.

### 2.2. Preparation of corrosion-resistant gas diffusion layer

An iridium–titanium nitride composite (Ir–TiN) was prepared as corrosion-resistant MPL by an ethylene glycol (EG) reduction method [24]. In this process, TiN nanoparticle (NanoAmor Inc., USA) was dispersed in EG (Sigma–Aldrich) and ultrasonically treated before drop-wise addition of $H_2IrCl_6$. NaOH (Mallinckrodt

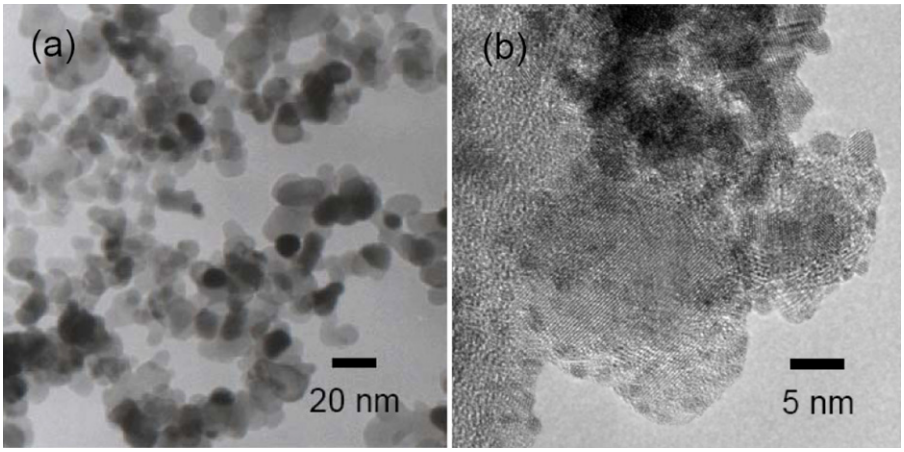


**Fig. 2.** The bright field TEM micrographs of (a) TiN and (b) Ir/TiN.

Chemicals) solution was added to control the size of Ir nanoparticles by adjusting the pH of the solution (>12). The solution was stirred well before heating at 160 °C for 3 h in nitrogen ($N_2$) atmosphere under refluxing conditions. When the solution was cooled down to room temperature, 1 M $H_2SO_4$ solution was used to reduce the pH to 2. The solution was stirred overnight and washed with copious amounts of DI water to remove any organic residues left due to the oxidation of EG. The prepared Ir–TiN was dried in air at 80 °C for 3 h.

Wet-proofed carbon paper (10 BC, SGL) was used as the gas diffusion backing (GDB). A suspension of 75 wt% Ir–TiN and 25 wt% polytetrafluoroethylene (PTFE) was sprayed onto the GDB to form the protective MPL. The process was repeated until the desired loading was achieved (0.5 mg $cm^{-2}$ of Ir–TiN). The corrosion-resistive GDL was obtained after sintering at 320 °C under $N_2$ atmosphere. The conventional GDL (10 BC, SGL) without the protective MPL was also tested under URFC conditions for comparison purpose.

### 2.3. Material characterization

Physical properties of Pt/$TiO_2$, Ir/$TiO_2$ and Ir–TiN were characterized by BET surface area analysis, X-ray diffraction (XRD), scanning electron microscopy (SEM), and transmission electron microscopy (TEM). BET surface area measurements were performed using a Quantachrome NOVA 2000 BET analyzer. XRD analysis was performed using a Rigaku X-ray diffractometer at $2\theta$ ranging between 20 and 80° using Cu-K$\alpha$ radiation. A tube voltage of 30 kV and a current of 15 mA were used during the scanning. Surface analysis of the bare and corrosion-resistant GDL was investigated using an FEI Quanta 200 Environmental Scanning Electron Microscope. TEM was carried out using a JEOL-2100F microscope equipped with a field emission electron gun source and operated at 200 kV. The metal loading of Pt and Ir deposited on the $TiO_2$ support was determined by inductively coupled plasma atomic emission spectrometry (ICP-AES).

### 2.4. Electrochemical characterization

The electrochemical properties of the supported catalysts were characterized by cyclic voltammetry (CV) and linear sweep voltammetry (LSV) techniques. All the electrochemical characterization studies were performed in 0.5 M $H_2SO_4$ using a Pine bipotentiostat (Model AFCBP1), a Pt-wire counter electrode, and an $Hg/Hg_2SO_4$ reference electrode [0.68 V vs. reversible hydrogen electrode (RHE)]. A rotating disk electrode (RDE) with a glassy carbon disk (0.247 $cm^2$) was used as the working electrode for studying the oxygen reduction reaction (ORR). In order to prevent the damage of the glassy carbon disk at high positive potential (>1.8 V), a Pt disk electrode (0.164 $cm^2$) was used during oxygen evolution reaction (OER) measurement. The catalyst ink (4 $mg_{catalyst}$ $mL^{-1}$) was prepared by blending the catalyst powder (supported or unsupported catalysts) with ethanol in an ultrasonic bath. The required amount of the catalyst ink was deposited onto the disk using a micro pipette. After drying, 5 μL of Nafion solution (0.25 wt.% Nafion) was added on top of the catalyst layer to minimize anion adsorption effects on the catalysts. All the potential values mentioned in the RDE study are referred to an RHE.

The ECSA of Pt was determined by charge integration under the hydrogen desorption peaks in the cyclic voltammograms appearing between 0 and 0.35 V, by assuming a charge of 210 μC $cm^{-2}$ for the electroactive Pt surface. Then, the specific ECSA was calculated based on the following relation:

$$\text{specific ECSA} = \frac{Q_H}{m \times q_H} \quad (2)$$

where $Q_H$ is the charge for hydrogen desorption, m is the loading amount of metal, and $q_H$ is the charge required for desorbing a monolayer of hydrogen on a Pt surface.

### 2.5. Unitized regenerative fuel cell operation

A commercially available catalyzed gas diffusion layer (GDL; LT140EW Low Temperature ELAT®GDE Microporous Layer, BASF) with and without the corrosion-resistant protective MPL was used as the bifunctional hydrogen electrode for the URFC experiments. The hydrogen electrode catalyst loading was 0.5 $mg_{Pt}$ $cm^{-2}$. The BOE catalyst ink was prepared by ultrasonically blending 0.15 g of Pt–Ir/$TiO_2$ or Pt–Ir black (Pt black: HiSPEC 1000, Alfa Aesar; Ir black: Alfa Aesar) catalyst powders with a Nafion solution (5 wt%, Alfa Aesar) and ethanol for 4 h. The catalyst ink was then sprayed onto the GDL (ELAT LT1400 W, BASF). The process was repeated until the desired metal loading was achieved (1.0 $mg_{Pt-Ir}$ $cm^{-2}$ for both Pt–Ir/$TiO_2$ and Pt–Ir black). The electrodes were hot-pressed onto both sides of a Nafion® NRE-212 membrane at 140 °C and 200 $psi_{abs}$ for 3 min. The MEA was then cooled and assembled in a single URFC for performance evaluation.

The performance of BOEs with Pt–Ir electrocatalysts for URFC was tested using a 5 $cm^2$ single cell with platinum coated titanium bipolar plates [25]. For the fuel cell testing, $H_2$ and $O_2$ humidified at 75 °C were supplied to the anode and cathode compartments, respectively; each at a flow rate of 150 mL $min^{-1}$. Polarization experiments were conducted using a fully automated test station (Fuel Cell Technologies Inc.) at 75 °C. No backpressure was applied during fuel cell operation. In the electrolyzer mode, de-ionized water heated at 80 °C was supplied to the BOE at a constant flow rate of 20 mL $min^{-1}$. The polarization curves of the water electrolysis were galvanostatically measured using a power supply. The cycle performance of the URFCs was investigated at constant voltage conditions. During cycling test, a constant voltage of 0.7 and 1.5 V was applied to cell during fuel cell (2 h) and water electrolysis mode (4 h), respectively.

## 3. Results and discussion

### 3.1. Physical characterization

The transmission electron microscope (TEM) images of $TiO_2$, Pt/$TiO_2$, and Ir/$TiO_2$ are shown in Fig. 1. Aggregation of granular $TiO_2$ was observed in the HRTEM image (Fig. 1a). The particle size of the synthesized $TiO_2$ particles was in the range between 7 and 15 nm with a BET surface area of 250 $m^2$ $g^{-1}$. The TEM image shown in Fig. 1b reveals the successful deposition of Pt particles onto the $TiO_2$ support. The average particle size of the Pt ($d_{Pt}$) is $d_{Pt}$ = 4.2 nm. Fig. 1c exhibits the TEM micrographs of well-distributed Ir particles on the $TiO_2$ support. The average size of the iridium particles ($d_{Ir}$) is found to be 2.0 nm. TEM results revealed that the Pt and Ir nanoparticles are uniformly distributed on the $TiO_2$ surface using the modified borohydride reduction method.

TEM analysis of the TiN and Ir–TiN samples is shown in Fig. 2. The average particle size of TiN is 20 nm with a BET surface area of 47 $m^2$ $g^{-1}$ whereas, the volume/area average particle size of the Ir ($d_{Ir}$) is calculated to be Ir = 2 nm based on a histogram of the Ir particle size distribution derived from the TEM measurements.

The scanning electron microscope (SEM) images of conventional GDL and corrosion-resistant GDL are shown in Fig. 3. The conventional GDL displays uniform surface contains many pores with diameters > 100 nm and a few pores in micrometer range (Fig. 3a). On the other hand, the corrosion-resistant GDL is denser than the carbon GDL as shown in Fig. 3b.

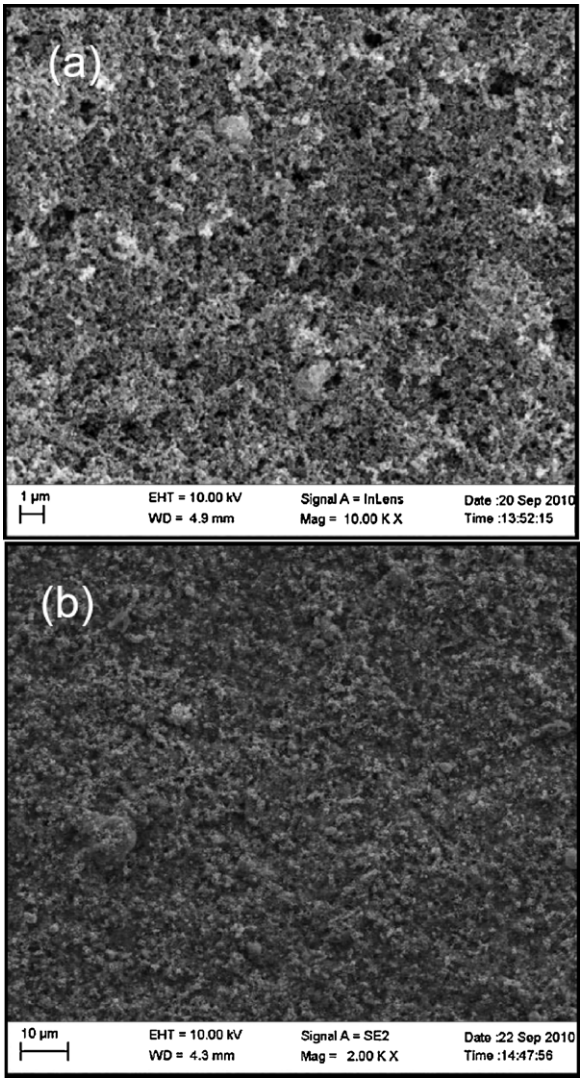


**Fig. 3.** SEM images of (a) conventional GDL and (b) corrosion-resistive GDL.

### 3.2. Electrochemical studies

The electrochemical activities of supported Pt and Ir catalysts towards oxygen reduction reaction (ORR) and oxygen evolution reaction (OER) were studied using linear sweep voltammetry technique (Fig. 4). The results indicated that the preferred oxygen reduction catalyst, Pt, demonstrated poor catalytic activity for OER. On the other hand, the preferred oxygen evolution catalyst, Ir, demonstrated poor activity for ORR. Therefore, it is suggested that an optimum amounts of these two catalysts should be identified in order to achieve a comparable ORR and OER characteristics to that of pure Pt and Ir catalysts, respectively. Therefore, physical mixtures of $Pt/TiO_2$ and $Ir/TiO_2$ catalysts with Pt:Ir compositions varying from 100:0 to 70:30 were prepared and their electrochemical performance as BOE electrocatalysts was studied.

Fig. 5a shows the polarization curves of ORR for the various Pt–Ir compositions. The ORR curves were under mixed kinetic-diffusion control reaction in the potential region between 0.95 V and 0.60 V, followed by a region where the diffusion limiting current ($\sim$3.5 mA cm$^{-2}$) was observed. The difference in the limiting currents for different catalysts may be attributed to the surface coverage of the catalyst and the physical properties such as the porosity of the thin catalyst layer deposited on the glassy carbon electrode. Furthermore, the $Pt_{70}Ir_{30}$ catalyst showed the lowest activity for oxygen reduction due to lower activity of the Ir catalyst for ORR. Fig. 5b shows the OER reactivity of Pt–$Ir/TiO_2$ catalysts as a function of catalyst composition. The onset potential for OER ($E_o$) for the $Pt_{100}Ir_0$ catalyst is approximately 1.55 V, while the $E_o$ for the $Pt_{70}Ir_{30}$ catalyst is approximately 130 mV more negative than the pure Pt catalyst. The OER studies indicated that among the various Pt–$Ir/TiO_2$ composite catalysts, the oxygen evolution rate significantly increased with the increase of Ir content up to 30 wt.%.

The catalyst efficiency ($\varepsilon$) under ORR and OER testing was calculated using Eq. (3):

$$\varepsilon\ (\%) = \frac{V_{ORR}}{V_{OER}} \times 100 \tag{3}$$

where $V_{ORR}$ and $V_{OER}$ is the voltage for the oxygen reduction and oxygen evolution reactions, respectively, at a given current density. Table 1 summarizes the efficiency of Pt–$Ir/TiO_2$ catalysts at a current density of 1.5 mA cm$^{-2}$. These results were obtained using RDE studies which indicated that the composite Pt–$Ir/TiO_2$ catalyst with Ir content of 15% showed higher catalytic efficiency than the other ratios, and therefore was used for further URFC studies.

### 3.3. Unitized regenerative fuel cell studies

The performance of Pt–Ir electrocatalysts as BOEs was evaluated using a 5 cm$^2$ single cell employing surface modified titanium bipolar plates [11,25]. Fig. 6 shows the polarization curves of the URFC using supported Pt–$Ir/TiO_2$ and unsupported Pt–Ir black as bifunctional oxygen catalysts. In the fuel cell mode (Fig. 6a), the Pt–$Ir/TiO_2$

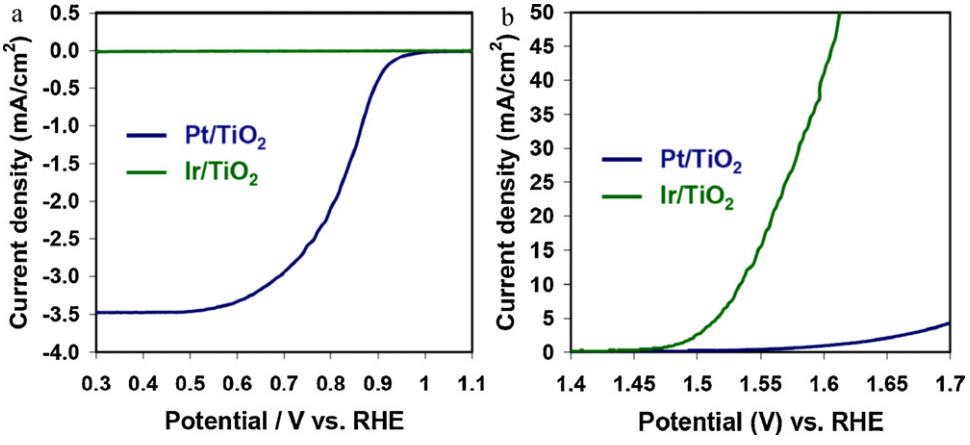


**Fig. 4.** (a) ORR and (b) OER polarization curves of the $Pt/TiO_2$ and $Ir/TiO_2$ electrocatalysts recorded at room temperature in 0.5 M $H_2SO_4$ solution with a sweep rate of 5 mV s$^{-1}$.

**Table 1**
Comparison of ORR and OER performances as a function of various compositions for the Pt–Ir/$TiO_2$ electrocatalysts.

| Catalyst | $V_{ORR}$ [a] (V) | $V_{OER}$ [a] (V) | $\varepsilon$ (%) |
|---|---|---|---|
| $Pt_{100}Ir_0$ | 0.846 | 1.629 | 51.9 |
| $Pt_{95}Ir_{05}$ | 0.840 | 1.548 | 54.3 |
| $Pt_{90}Ir_{10}$ | 0.834 | 1.524 | 54.7 |
| $Pt_{85}Ir_{15}$ | 0.830 | 1.504 | 55.2 |
| $Pt_{80}Ir_{20}$ | 0.822 | 1.493 | 55.1 |
| $Pt_{75}Ir_{25}$ | 0.818 | 1.488 | 55.0 |
| $Pt_{70}Ir_{30}$ | 0.816 | 1.486 | 54.9 |

[a] $V_{ORR}$ and $V_{OER}$ is the voltage for the oxygen reduction reaction and oxygen evolution reaction, respectively, at current density of 1.5 mA $cm^{-2}$.

electrocatalyst generated 1.38 A $cm^{-2}$ at 0.60 V and a maximum power density of 0.93 W $cm^{-2}$. As can be seen from the figure, much lower performance was obtained for the Pt–Ir black electrode due to the large and aggregated catalyst particles of the unsupported catalysts. The current density at 0.6 V is 0.74 A $cm^{-2}$, which is approximately half of that obtained when employing Pt–Ir/$TiO_2$ as the catalyst. In the water electrolyzer mode (Fig. 6b), the performance of supported Pt–Ir/$TiO_2$ is higher than that of unsupported Pt–Ir black. These values are much higher than the values obtained for Pt and Ir black BOE catalysts reported in the literature [17,18]. With the increase in the operating current density, the difference in cell voltage between the supported and the unsupported catalyst at a particular current density was also increased.

Based on voltage and current density relationship, the energy conversion efficiency of fuel cell ($\varepsilon_{FC}$) and water electrolysis ($\varepsilon_{WE}$) can be calculated using the following equations [26]:

$$\varepsilon_{FC}\ (\%) = \frac{nFV_{FC}}{\Delta H} \times 100 \quad (4)$$

$$\varepsilon_{WE}\ (\%) = \frac{\Delta H}{nFV_{WE}} \times 100 \quad (5)$$

where $n$ is the number of moles of electrons involved in the reaction, $F$ is the Faraday constant, $\Delta H$ is the higher heating values (HHV) of enthalpy change for the reaction, $V_{FC}$ and $V_{WE}$ are the voltages for the fuel cell and water electrolysis at a given current density. The round-trip energy conversion efficiency ($\varepsilon_{RT}$) can be obtained by multiplying Eqs. (4) and (5) [6]:

$$\varepsilon_{RT}\ (\%) = \frac{V_{FC}}{V_{WE}} \times 100 \quad (6)$$

Fig. 7 depicts the comparison of efficiencies of Pt–Ir black and Pt–Ir/$TiO_2$ catalysts at various operating current densities and the $\varepsilon_{FC}$, $\varepsilon_{WE}$, and $\varepsilon_{RT}$ values are summarized in Table 2. As can be seen from the figure, the URFC efficiency of Pt–Ir/$TiO_2$ catalyst is much higher than the Pt–Ir black catalyst at all current densities. The $\varepsilon_{RT}$ of Pt–Ir black was 42.4% and 29.8% at 0.5 and 1.0 A $cm^{-2}$, respectively. In contrast, the high $\varepsilon_{RT}$ observed for Pt–Ir/$TiO_2$ indicated

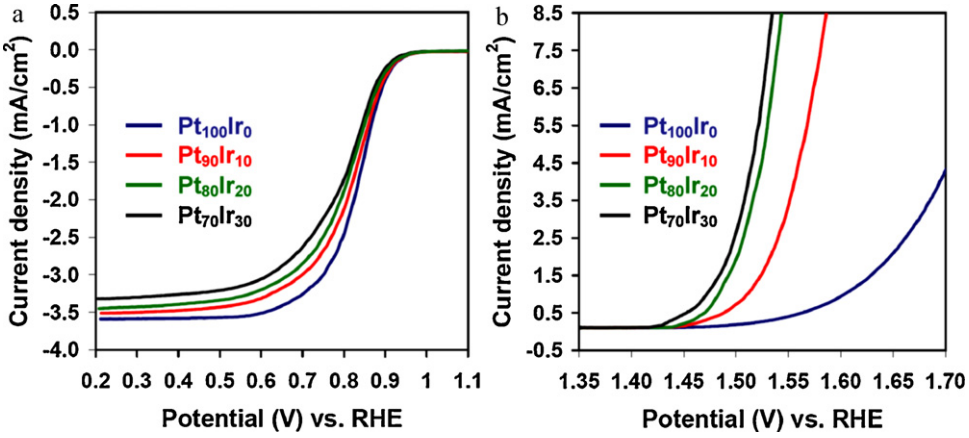


**Fig. 5.** (a) ORR and (b) OER polarization curves as a function of Pt–Ir compositions for the Pt–Ir/$TiO_2$ electrocatalysts. The experiment was performed at room temperature in 0.5 M $H_2SO_4$ solution with a sweep rate of 5 mV $s^{-1}$ and a rotation rate of 900 rpm. The metal loading on the electrode was 90 and 100 μg $cm^{-2}$ for ORR and OER, respectively.

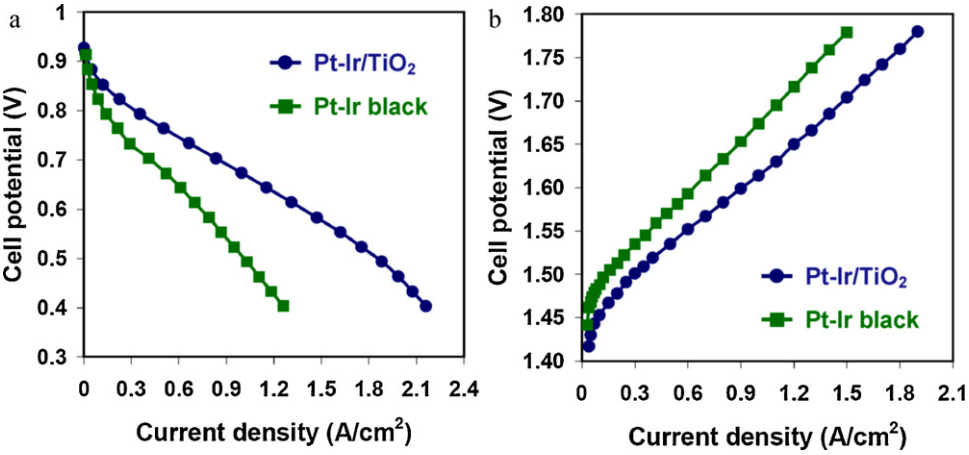


**Fig. 6.** Polarization curves of the PEM. (a) Fuel cells and (b) water electrolyzers with the Pt–Ir/$TiO_2$ and Pt–Ir black bifunctional oxygen electrode catalysts. Catalyst loading at hydrogen electrode: 0.5 $mg_{Pt}$ $cm^{-2}$; catalyst loading at oxygen electrode: 1.0 $mg_{Pt-Ir}$ $cm^{-2}$ (Pt/Ir = 85/15); $H_2$ and $O_2$ flow rates: 150 mL $min^{-1}$; humidity: 100%RH; $H_2O$ flow rate: 20 mL $min^{-1}$; cell temperature: 80 °C.

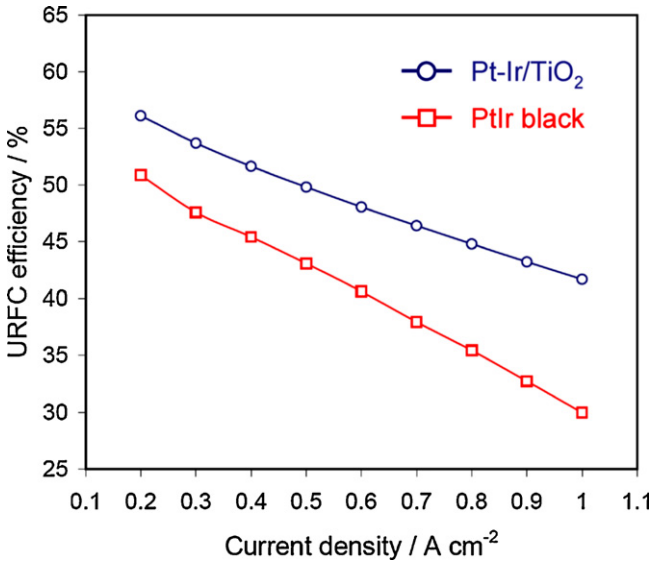


**Fig. 7.** URFC round-trip energy conversion efficiencies as function of current density using Pt–Ir/$TiO_2$ and Pt–Ir black as bifunctional oxygen catalysts.

**Table 2**
Voltage and efficiency of URFCs at 0.5 and 1.0 A $cm^{-2}$ by employing Pt–Ir/$TiO_2$ and Pt–Ir black as bifunctional oxygen electrocatalysts.

| Catalyst | Loading[a] ($mg_{Pt-Ir}$ $cm^{-2}$) | Current density (A $cm^{-2}$) | $\varepsilon_{FC}$ (%) | $\varepsilon_{WE}$ (%) | $\varepsilon_{RT}$ (%) |
|---|---|---|---|---|---|
| Pt–Ir/$TiO_2$ | 1.0 | 0.5 | 52.0 | 96.7 | 50.3 |
| Pt–Ir black | 1.0 | 0.5 | 45.3 | 93.7 | 42.4 |
| Pt–Ir/$TiO_2$ | 1.0 | 1.0 | 45.9 | 91.9 | 42.2 |
| Pt–Ir black | 1.0 | 1.0 | 33.8 | 88.1 | 29.8 |
| Pt–Ir black | 2.0 | 1.0 | 41.9 | 89.2 | 37.3 |

[a] Catalyst loading on the bifunctional oxygen electrode.

that it is electrochemically more active than Pt–Ir black. The $\varepsilon_{RT}$ of URFC is enhanced by 7.9% and 12.4% at 0.5 and 1.0 A $cm^{-2}$, respectively, when using the Pt–Ir/$TiO_2$ as bifunctional oxygen catalyst. Furthermore, the URFC performance of Pt–Ir/$TiO_2$ at a metal loading of 1.0 mg $cm^{-2}$ is much higher than that of Pt–Ir black employed at 2.0 mg $cm^{-2}$ on the oxygen electrode (Table 2).

Table 3 summarizes the particle size and ECSA of supported and unsupported electrocatalysts. The present studies indicated that the $TiO_2$ support provides high surface area for the better dispersion of metal particles. As a result of the support effect, the Pt/$TiO_2$ ($d_{Pt}$ = 4.2 nm) and Ir/$TiO_2$ ($d_{Ir}$ = 2.0) showed a smaller

**Table 3**
Summary of particle size and ECSA of supported and unsupported electrocatalysts.

| Catalyst | Particle size (nm) | ECSA ($m^2$ $g^{-1}$) |
|---|---|---|
| Pt/$TiO_2$ | 4.2 | 30.5 |
| Ir/$TiO_2$ | 2.0 | – |
| Pt black | 6.6 | 14.8 |
| Ir black | 10–50 | – |

catalyst particle size than the unsupported Pt ($d_{Pt}$ = 6.6 nm) and Ir ($d_{Ir}$ = 10–50 nm), respectively. The ECSA of Pt is 30.5 and 14.8 $m^2$ $g^{-1}$ for Pt/$TiO_2$ and Pt black, respectively. Therefore, the increase in the URFC performance was ascribed to the better utilization of catalyst particles on the $TiO_2$ support. It is important to note that a high noble metal loading (typically 8–10 mg $cm^{-2}$) has been used in URFC catalysts layers [13]. The high performance of the Pt–Ir/$TiO_2$ electrocatalyst synthesized in this investigation offers a new approach to decrease the catalyst loading with the help of a highly stable supported bifunctional oxygen electrode catalyst.

### 3.4. Cycling test

Fig. 8 shows the performance stability of the unit cell employing GDLs with MPLs made of carbon and Ir–TiN after the operation of the cell at 2.0 V for 1 h every day. Polarization measurements in fuel cell mode were performed after operating the cell at 2.0 V. As shown in Fig. 7a, the unit cell with carbon-based MPL shows poor stability after the operation of the unit cell in extreme corroding conditions. This is mainly due to the corrosion of the carbon MPL which lead to the increased contact resistance and severe water flooding. As shown in Fig. 8b, the unit cell with the Ir/TiN MPL exhibits much better stability than that with carbon-based MPL after the operation of unit cell for 20 cycles. Since there is no corrosion on the surface of Ir-Ti MPL, the main reason for performance degradation in the polarization curve is probably the degradation of the bipolar plates. In spite of the degradation of the material in the MEA at the severe corroding conditions, the stability of unit cell performance was significantly improved by the Ir–TiN protecting layer by suppressing the corrosion of underlying carbon MPL.

Based on the polarization stability data of the unit cell with Ir–TiN protecting layer, a short-term cycling test of the URFC was carried out in both fuel cell and electrolyzer mode for 36 h at 0.7 and 1.5 V, respectively, as shown in Fig. 9. The potentials of the URFC were kept at 0.7 and 1.5 V in fuel cell mode and electrolyzer mode, respectively. As can be seen from the figure, the current density of 0.7 and 0.4 A $cm^{-2}$ was achieved in fuel cell and water electrolyzer mode, respectively for 36 h. The slight performance degradation

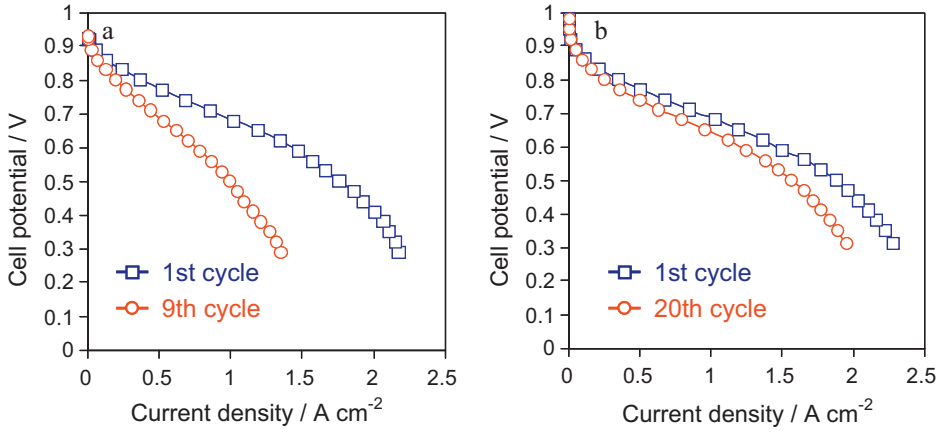


**Fig. 8.** Comparison of the stability of unit cell performance after the cycling operation of cell at 0.7 and 1.5 V for 2 h with (a) carbon-based MPL and (b) Ir–TiN MPL.

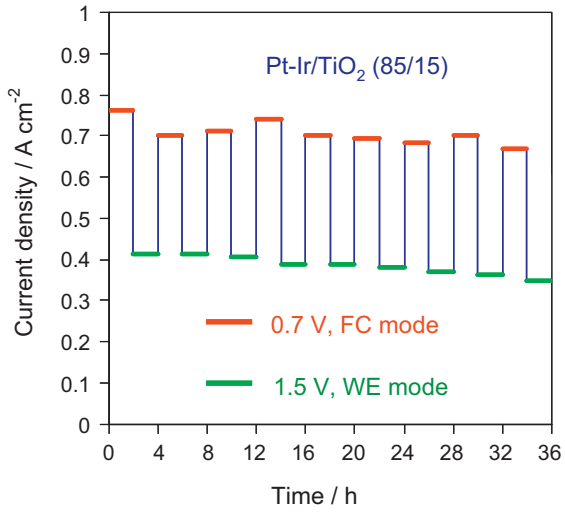


**Fig. 9.** Short-term cycling performance of URFC employing Pt–Ir/$TiO_2$ as bifunctional oxygen catalyst and Ir–TiN microporous layer.

in water electrolyzer mode can be attributed to the degradation in the bipolar plates due to increased resistance. However, the short-term stability studies of $TiO_2$ supported Pt–Ir catalyst and the Ir–TiN based MPL in both fuel cell mode and electrolyzer mode is very promising and can be considered for application as BOE and corrosion resistant MPL, respectively in URFCs.

## 4. Conclusion

In this study, Pt/$TiO_2$ and Ir/$TiO_2$ electrocatalysts were synthesized and their physical mixture was investigated as BOE catalyst for URFC application. The performance of Ir–TiN was evaluated and the results suggested that it can be employed as a corrosion-resistant microporous layer. The URFC testing results indicated a substantial improvement in round-trip efficiency for the supported Pt–Ir/$TiO_2$ (42.2%) when compared to that obtained for the unsupported Pt–Ir black (29.8%). Furthermore, the Pt–Ir/$TiO_2$ catalyst showed higher URFC performance at a metal loading of 1.0 mg $cm^{-2}$ when compared to that of Pt–Ir black catalyst at 2.0 mg $cm^{-2}$ loading on the oxygen electrode. The increase in the URFC performance was attributed to the support effect by providing a high surface area for uniform dispersion and better utilization of the catalyst particles.

## Acknowledgements

The financial supports of National Science Foundation (CBET – 0966956) and NASA-EPSCoR (NNX07AT68A) are gratefully acknowledged.

## References

[1] T.W. Patterson, R.M. Darling, Electrochem. Solid-State Lett. 9 (2006) A183–A185.
[2] G.Y. Chen, S.R. Bare, T.E. Mallouk, J. Electrochem. Soc. 149 (2002) A1092–A1099.
[3] J. Pettersson, B. Ramsey, D. Harrison, J. Power Sources 157 (2006) 28–34.
[4] L. Jorissen, J. Power Sources 155 (2006) 23–32.
[5] F. Mitlitsky, B. Myers, A.H. Weisberg, Energy & Fuels 12 (1998) 56–71.
[6] H.Y. Jung, S. Park, B.N. Popov, J. Power Sources 191 (2009) 357–361.
[7] R.N. Singh, D. Mishra, Anindita, A.S.K. Sinha, A. Singh, Electrochem. Commun. 9 (2007) 1369–1373.
[8] S.Y. Huang, P. Ganesan, B.N. Popov, Appl. Catal. B 93 (2009) 75–81.
[9] T. Ioroi, Z. Siroma, N. Fujiwara, S. Yamazaki, K. Yasuda, Electrochem. Commun. 7 (2005) 183–188.
[10] S.D. Song, H.M. Zhang, X.P. Ma, Z.G. Shao, Y.N. Zhang, B.L. Yi, Electrochem. Commun. 8 (2006) 399–405.
[11] H.Y. Jung, S.Y. Huang, P. Ganesan, B.N. Popov, J. Power Sources 194 (2009) 972–975.
[12] S.S. Dihrab, K. Sopian, M.A. Alghoul, M.Y. Sulaiman, Renew. Sust. Energy Rev. 13 (2009) 1663–1668.
[13] U. Wittstadt, E. Wagner, T. Jungmann, J. Power Sources 145 (2005) 555–562.
[14] H. Chhina, D. Susac, S. Campbell, O. Kesler, Electrochem. Solid-State Lett. 12 (2009) B97–B100.
[15] K. Kinoshita, Carbon: Electrochemical and Physicochemical Properties, John Wiley & Sons, New York, 1988.
[16] P. Millet, R. Ngameni, S.A. Grigoriev, V.N. Fateev, Int. J. Hydrogen Energy 36 (2011) 4156–4163.
[17] S.A. Grigoriev, P. Millet, V.I. Porembsky, V.N. Fateev, Int. J. Hydrogen Energy 36 (2011) 4164–4168.
[18] S.A. Grigoriev, P. Millet, K.A. Dzhus, H. Middleton, T.O. Saetre, V.N. Fateev, Int. J. Hydrogen Energy 35 (2010) 5070–5076.
[19] L.R. Ma, S. Sui, Y.C. Zhai, J. Power Sources 177 (2008) 470–477.
[20] G.Y. Chen, C.C. Waraksa, H.G. Cho, D.D. Macdonald, T.E. Mallouk, J. Electrochem. Soc. 150 (2003) E423–E428.
[21] T. Ioroi, T. Oku, K. Yasuda, N. Kumagai, Y. Miyazaki, J. Power Sources 124 (2003) 385–389.
[22] S.Y. Huang, P. Ganesan, S. Park, B.N. Popov, J. Am. Chem. Soc. 131 (2009) 13898–13899.
[23] B. Avasarala, T. Murray, W.Z. Li, P. Haldar, J. Mater. Chem. 19 (2009) 1803–1805.
[24] Z.W. Chen, L.B. Xu, W.Z. Li, M. Waje, Y.S. Yan, Nanotechnology 17 (2006) 5254–5259.
[25] H.Y. Jung, S.Y. Huang, B.N. Popov, J. Power Sources 195 (2010) 1950–1956.
[26] J. Laminie, A. Dicks, Fuel Cell Systems Explained, Wiley, 2003, pp. 34–35.